RSC Advances

ROYAL SOCIETY OF CHEMISTRY

www.rsc.org/advances

Table of Contents

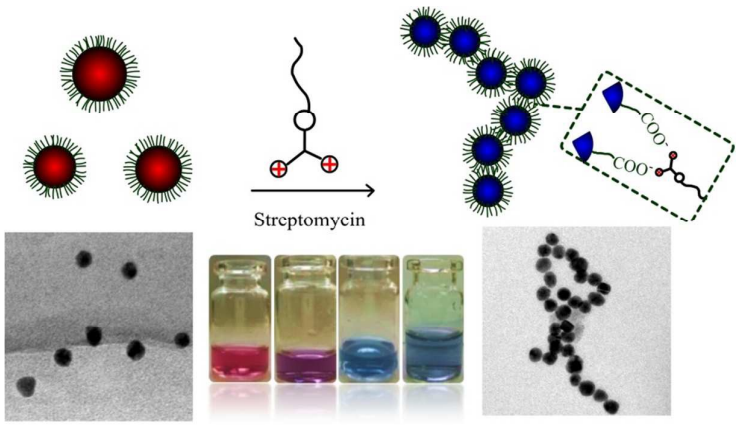

The disperse PMMA-@-AuNPs particles turn to chain-like arrays driven by electrostatic dipole interaction between two amino groups of AMGs and carboxylic group. The process shows a distinct color change companied the rise of zeta-potentials.

Constructing One Dimensional Assembly of Poly Methylacrylic Acid Capping Gold Nanoparticles for Selective and Colorimetric Detection of Aminoglycoside antibiotics

Junbo Li ·Ke Zhang ·Liang Ju·Wenlan Wu·Jinwu Guo·Huiyun Zhou

Here, a self-assembly driven colorimetric method is described for detecting aminoglycoside antibiotics (AMGs) upon nanochain formation of Poly methylacrylic acid capping gold nanoparticle (PMMA-@-Au NPs). After addition of streptomycin, the development of new plasmonic coupling absorption in the higher-wavelength region, companied with a prominent color change from wine red to blue, and TEM observation clearly reveal formation of chain-like nanostructure of PMMA-@-Au NPs. The amine-groups on AMGs can serve as a molecular bridge for electrostatic coupling with two carboxylic acids from adjacent particles to drive PMMA-@-Au NPs with chain-like arrays, where the molecular linkers are also target analytes. The selective detection can be achieved by the UV spectra of AMGs, including gentamicin, neomycin and kanamycin, with other types of antibiotics. Finally, the interference from metal ions competition can be eliminated by adding a strong metal ion chelator such as EDTA.

Introduction

As a large group of pharmaceuticals, antibiotics drug have been widely used for the abatement of bacterial infections with humans and animals[1]. Recently, animal

* Corresponding authors at: College of Chemical Engineering & Pharmaceutics, Henan University of Science & Technology, Luo Yang, China, 471023.

E-mai l addresses: Lijunbo@haust.edu.cn (J.B. Li);

Tel: +86-379-64231914; Fax: +86-379-64232193.

husbandry also employed antibiotics as feed additives to prevent animal diseases in and promote growth in farm animals[2]. However, abuse of antibiotics has raised public health concerns, with regard to the presence of antibiotics residues in the food chain[3, 4]. These residues will cause a serious threat to human health[5], such as chemical poisoning, allergic reactions, change in consumer perception of the product and the development of mechanisms of bacterial resistance. So far, various approaches and techniques have been developed for the determination of these residues in food, such as enzyme-linked immunoassay[6], high-performance liquid chromatography[7, 8], and capillary electrophoresis[9]. These methods have revealed several advantages, such as low detection limit and high sensitivity. However, rely on tedious sample pretreatment, special instrumentation or time-consuming procedures that limit their applications in the real-time and in site monitoring. Therefore, exploration of inexpensive, convenient and rapid method is highly desirable for use in routine assays.

Gold nanoparticles (Au NPs) have raised considerable concerns for its wide application in molecule recognition due to their distinct physical and chemical properties[10-14]. The unique optoelectronic properties, including higher molar absorption coefficient in visible region and the surface plasma resonance (SPR) absorption depending on particle size, distance and surrounding environment, make them as excellent platform for colorimetric detection. Moreover, the easy modified surface provides optional strategies for binding with a wide range of organic and biological ligands, and specifically and selectively interacting with target analytes[15]. Commonly, the aggregation of particle triggers an obvious color change and spectrum response, which is easy for detection of target analytes by naked eyes or inexpensive instruments. The quantity of target analytes, time of response and distinctness of color change was related to the aggregate manner of Au NPs, further determining the testing sensitivity.

Recently, constructing ordered array of metal nanoparticles has become the promising strategy for developing next-generation nanotechnologies[16-18]. The one-dimensional (1D) nanostructures[19, 20] produced an electromagnetic focusing effect caused by the plasmon coupling, which is distinct properties different from a simple collection of

individual particles[21, 22] and achieved the potentials of isolated nanoparticles in nanoelectronics, optoelectronics, nanomagnetism and sensor devices[23-25]. Self-assembly approach is an efficient and attractive methodology to create such nanomaterials via designable surface chemistry[26] and reliable interactions[27, 28]. Especial through the electrostatic dipole interaction[29], the little amount charged molecular linker could rapidly induce ordered array of disperse Au NPs, giving rise to marked change in optoelectronic property. Accompanied the variations in absorption spectra and distinct color change of solutions, fabricating the nanostructure has been believed to be a development of chemical[30, 31] and biomolecular SPR[32, 33] sensors due to sensitive easy-to-visualize process. For example, Cheng et al. employed 1D arrangement of AuNPs for colorimetric detecting Hg^{2+} with high reliability and excellent selectivity[34]. Fernández-Lodeiro's group[35] self-assemblied silver nanoparticles (AgNPs) and AuNPs into 1D nanochains mediated by polyamine to explore the value for colorimetric detection. In addition, the chain-like nanostructures based on polymer functional Au NPs was also prepared by us, showing a potential utility as sensor to discriminate the polyvalent anions from its corresponding monovalent anion[36], where the polyvalent anions served as molecular linkers.

Here, we further explore this self-assembling driven method for colorimetric detecting aminoglycoside antibiotics (AMGs) through fabricating nanochains of Poly methylacrylic acid capped gold nanoparticle (PMMA-@-Au NPs) in aqueous solution. AMGs residues[37] have been found in animal organs, milk, fruit, honey and vegetables[38] because of their wide application in veterinary medicine and pesticide. Commonly, AMGs are difficult to directly detect due to lack of UV-absorbing chromophore[39]. However, AMGs have many amino groups in the streptamine rings[33, 40], presenting new approach to discriminate them from other types antibiotics. In this paper, the assembling PMMA-@-AuNPs particles into chain-like arrays can be driven by two amino groups of AMGs via an electrostatic dipole interaction, where AMGs is both the molecular linkers and target analytes. The process of preparing PMMA-@-AuNPs and forming chain-like nanostructure to detect streptamine is illustrated in Scheme 1.

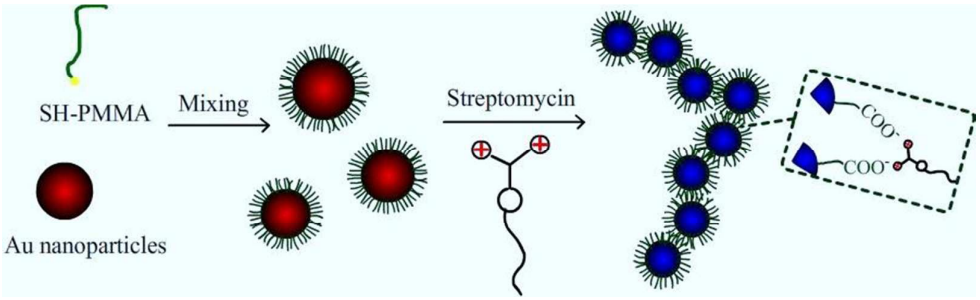

Scheme 1. Schematic representation of preparing PMMA-@-Au NPs and forming a chain-like nanostructure via electrostatic dipole interaction.

Experimental Section

Materials. The antibiotics gentamicin, streptomycin, neomycin, kanamycins, penicillin, tetracycline, terramycin and ilotycine were purchased from National Pharmaceutical Group Chemical Reagent. EDTA, and metal salts $Pb(NO_3)_2$ were purchased from National Pharmaceutical Group Chemical Reagent. All glassware was cleaned with freshly aqua regia and thoroughly rinsed with Mili-Q water prior to use. Au NPs were firstly prepared by using the classical citrate reduction method. PMAA-@-Au NPs was prepared by adding PMAA with a thiol end group ($SH\text{-}PMAA_{35}$) into the as-prepared Au NPs solution. The detail preparation and characterization of $SH\text{-}PMAA_{35}$, Au NPs and PMAA-@-Au NPs could find in our previous reference[14]. The Detailed description self-assembling Au NPs and PMAA-@-Au NPs by AMGs could find in support information.

Instrumentation. Transmission electron microscopy (TEM) is conducted by using a Philips T20ST electron microscopy at an acceleration voltage of 200kV. Thin films are prepared by dipping a drop of the solution onto a carbon-coated copper grid and then volatilizing the solution at room temperature. UV-vis absorption spectrum is obtained using a Perkin-Elmer UV-vis spectrometer (Lambda 20). Zeta-potentials were measured using a temperature-controlled Zetasizer 2000 (Malvern Instruments. Ltd.). The Au NPs and PMAA-@-Au NPs is characterized by dynamic laser scattering (DLS) for particle size analysis. DLS measurements are performed on a laser light scattering spectrometer (BI-200SM) equipped with a digital correlator

(BI-9000AT) at 532nm.

Results and Discussion

Characterizated of the PMMA-@-Au NPs.

Au NPs were firstly prepared by reducing chloroauric acid with sodium citrate. The PMMA-@-Au NPs could be achieved in one-step process simply by adding the SH-PMMA into an Au NPs aqueous solution via Au-S bond. The UV-vis spectroscopy was used to characterize the formation of Au-S covalent bonds on the surface of Au NPs. As shown in Fig. 1A, the characteristic SPR band of Au NPs is found in the spectrum at approximate 519 nm. After addition of the PMMA, the characteristic SPR band of PMMA-@-Au NPs moves to 524 nm. The UV absorption peak has red shift of 5nm. The slight red shift could be attributed to the change of the surface properties of Au NPs due to the chemisorption of PMMA on the surface of Au NPs, caused by the change of refractive index[30]. The existence of the polymer layer around the gold core can be directly observed by TEM image (Fig. 1B). The amorphous phase of grafted PMAA chains packs on the crystal structure gold core. The core has a mean diameter of approximately 13nm. The characterization of TGA and DLS can directly provide the information of the core-shell structure as shown in Fig. 1C and D. The average hydrodynamic diameter (D_h) of the particles is approximately 28nm, and the size distribution range is 25-34 nm. From the results of TEM and DLS, the mean length of the shell is approximately 7.5nm. From Fig. 1D, the PMMA is found to decompose in the temperature range from 285 to 448 °C. Thus, the weight percentage of PMMA is approximately 58%. Therefore, the average grafting density of PMMA on the surface of each Au NPs is approximately 1.02 chains/nm^2.[36]

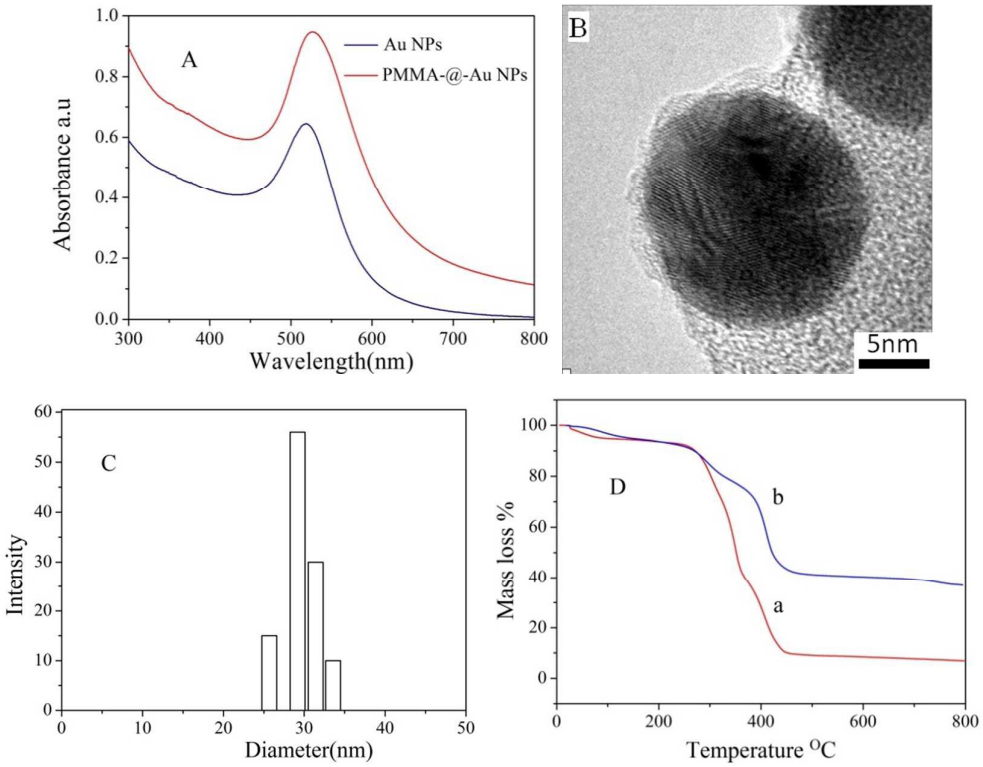

Fig. 1 UV-vis spectra (A) of Au NPs and PMMA-@-Au NPs, TEM (B) and DLS of PMMA-@-Au NPs(C), and TGA analysis (D) of PMMA(a) and PMMPImB-@-Au NPs (b).

Bearing two guanidinium cations in PBS buffer solution due to its pKa values up to 13.5, streptomycin can randomly associate with two carboxy groups via electrostatic interaction. The Fig.2 shows the evolution of SPR of PMMA-@-Au NPs after the addition of streptomycin with an increasing concentration. In this case, the streptomycin adds dropwise and the spectrum is measured after 15min incubation to ensure full interaction. With addition of streptomycin, the intensity of the transverse band at 523 nm declines. The second new SPR band in the higher wavelength region gradually appears, which attributes to the formation of aggregated nanostructures. The long-wavelength plasmon band is originated from the coupling of the plasmon resonance of neighbouring Au NPs. The intensity of the long-wavelength band increases with the increase the amount of streptomycin and finally reaches a plateau at 657nm at 30μL streptomycin. The longitudinal mode of plasmon oscillation is excited along with the formation of a longer chain. However, the blue suspension is observed

in the solution when increase the amount of streptomycin to 35 and 40μL, which makes the intensity of the long-wavelength band decline.

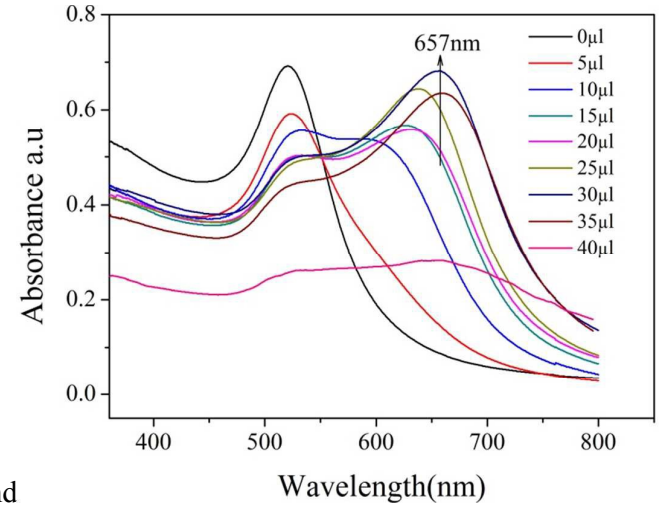

and

Fig. 2. UV -vis spectra of PMMA-@-Au NPs with the addition of different volumes of streptomycin.

The negative charge of particle surface makes the particles end-on alignment due to the electrostatic repulsive interaction[41, 42]. The formation of the nanochain is driven by a balance between two opposite interactions[43]. Their change trend can be analysed by the measurement particle surface potentials, showing in Fig. 3. From Fig. 3, the zeta-potentials of PMMA-@-Au NPs raises steadily because the addition of positive streptomycin partly neutralizes the negative charge of PMMA-@-Au NPs. The zeta-potentials rise from the original -24.2 to -1.3 mV after the addition of 35μl of streptomycin. With an increase in the amount of streptomycin, the decreased negative zeta-potential is caused by the occurrence of electrostatic dipole interaction. The color change along with change of zeta-potentials was inserted in the Fig. 3, which can be used to indicate the change of electrostatic interaction and formation of nanochain. The electrostatic repulsive interaction makes particles disperse well and show the red color. After addition of streptomycin, the electrostatic dipole interaction promotes the formation of nanchian, generating the absorbance in higher wavelength region and making the color change from red to purple and blue. At high streptomycin concentrations, the lower electrostatic repulsive interaction leads to the formation of the close-packed nanostructures, confirming by blue suspension in solution. The distinct change of color offers a reliable visual detection for streptomycin. The

recognizable concentration for streptomycin is 11.6ppb with naked eye, which is lower than maximum residue limits (MRL) for streptomycin in milk defined by European Union, America, China, and WHO (200 ppb) [44].

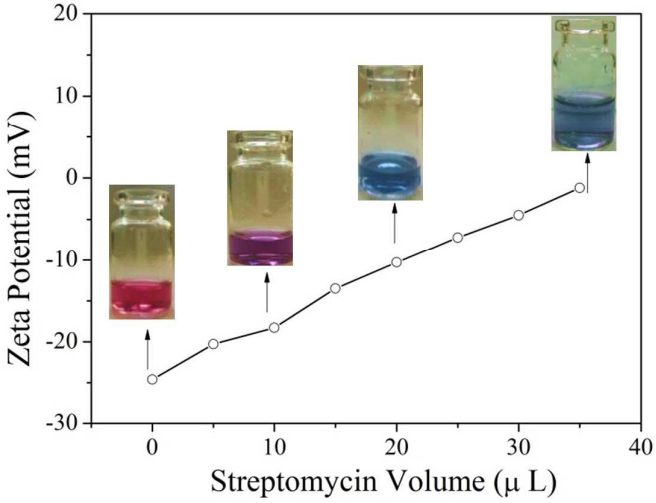

Fig.3. Zeta-potentials and photos of PMMA-@-Au NPs in the presence of different volume streptomycin.

The time-dependent optical spectra (Fig. 4) were also studied by directly added the 30μL of streptomycin into the solution of PMMA-@-Au NPs. From Fig. 4, the aggregate nanstructures can be fully assembled within 12min and the solution keeps generally stable for days without the observation of manifest precipitation. The guanidinium group can fast bind with carboxyl group through electrostatic attraction, which provides a rapid detection for streptomycin.

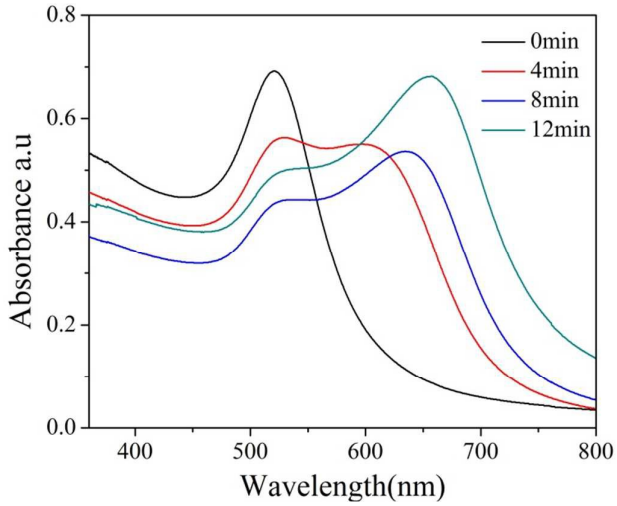

Fig. 4. Time-dependent UV-vis spectra of PMMA-@-Au NPs at various times after

addition of 30μL of streptomycin.

The TEM images of PMMA-@-Au NPs in the absence and presence of different concentrations of streptomycin clearly confirm the self-assembled process of gold nanochain formation. From Fig. 5a, the particles disperse well because of the electrostatic repulse among the carboxylate ions in absence of streptomycin as molecular linker. After added 5μL streptomycin, the short chains of PMMA-@-Au NPs are found in the image Fig. 5b. The higher electrostatic repulsive interactions prevent the formation of long-chain structure. With the increasing amount of streptomycin in solution, the nanochains grow longer because more molecular linkers take part in self-assembly (Fig. 5c). The long chains are flexible due to a random electrostatic interaction. Continuing to increase the amount of streptomycin, as shown in Fig. 5d and e, the chains with branch and close-packed structure are observed since the continuous decrease of electrostatic repulsive interaction.

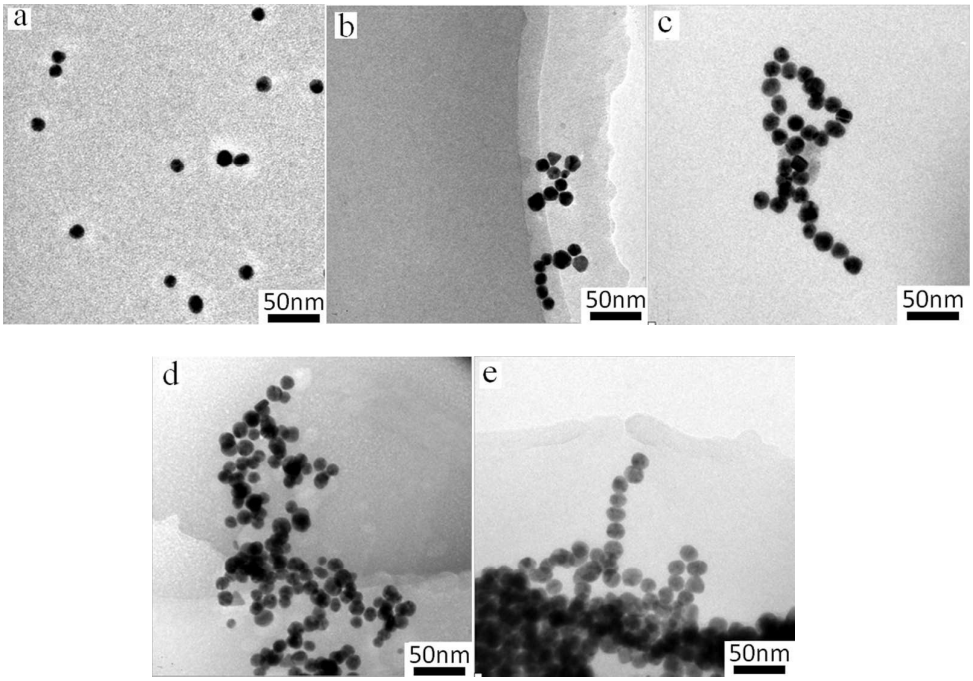

Fig.5.TEM images of PMMA-@-Au NPs in the absence (a) and presence of 5μl (b), 10μl (c), 20μl (d) and 30μl (e) streptomycin.

Actually, the citrate-stabilized Au NPs has been widely reported to construct

multi-dimensional self-assemblies via electrostatic interaction with cationic coupling agent[45]. Here, the formation of self-assembling Au NPs was also verified to visually detect streptomycin. The second new SPR band in the higher wavelength region(Fig. 6a) is observed after addition of streptomycin in the solution of Au NPs, confirming the formation of aggregated nanostructures. The longitudinal mode of plasmon band finally locates at 666nm after adding 15μl of streptomycin. Compared with PMMA-@-Au NPs, a little redshift plasmon band indicates a shorter distance between adjacent particles. The clear color change from red to blue can also be used for detecting streptomycin with naked eyes. However, lower intensity and wider peak suggests an unstable and irregular structure. The TEM image (Fig. 6b) reveals a part fusion of nanstructure. The nanstructures remain chain-like tendency, indicating particles coalescence occur after the electrostatic self-assembly, which attributes to ineffective protection from citrate noncovalent coating surface. The results indicate that the polymer shell not only provides functional group to interact with AMGs, but stability to prevent Au NPs from coalescence between particles.

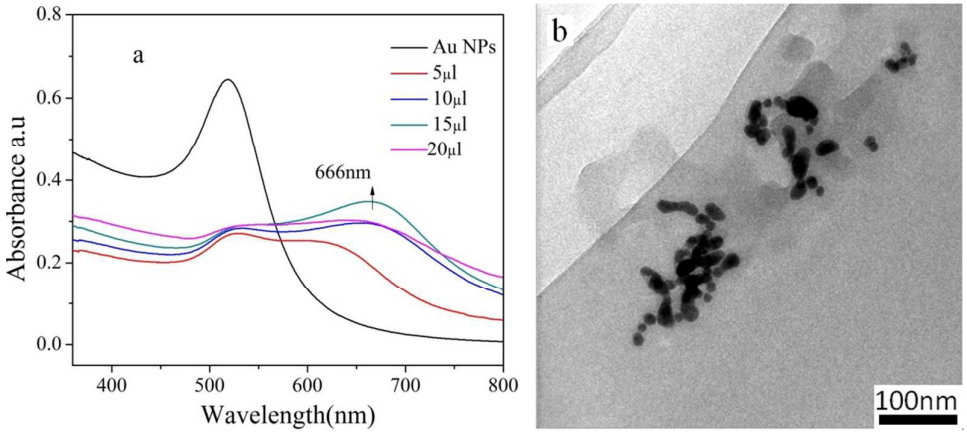

Fig. 6. UV -vis spectra of citrate-stabilized Au NPs with the addition of different volumes of streptomycin and TEM image of citrate-stabilized Au NPs in the presence of 15μl streptomycin.

The others AMG, including gentamicin, neomycin and kanamycin, with several amine-groups on molecular skeleton, have potential ability to induce linear self-assembly of PMMA-@-Au NPs via electrostatic interaction. Here, we compared the UV-vis spectra of PMMA-@-Au NPs in the presence of the same concentrations

of AMG and other types of common antibiotics, as shown in Fig. 7. Fig. 7a shows the UV-vis spectra of the PMMA-@-Au NPs after adding streptomycin, gentamicin, neomycin and kanamycin. From Fig. 7a, besides the transverse SPR band at 524 nm, the longitudinal SPR band at 623-662nm is also found in those spectra, and TEM image confirming the formation of chain-like Au NPs by TEM (Fig.1s). The protonated amino groups can also be used as the linkers among PMMA-@-Au NPs to induce a particles order aggregation. The different absorbance intensity of longitudinal SPRs maybe is caused by the number of amino group and different molecule property. All the colors of solution turn to blue, illustrating the feasibility of colorimetric detection. Fig. 7b shows the UV-vis spectra of the PMMA-@-Au NPs after addition of other types of common antibiotics, including penicillin, terramycin, tetracycline and ilotycin, etc. From Fig. 7b, the transverse SPRs remain in the same position, showing that those antibiotics lack the ability to interact with PMMA-@-Au NPs. The formation of chain-like Au NPs is induced by electrostatic dipole interaction, instead of via a hydrogen-bonding. Therefore, the self-assembly driven colorimetric method can serve to distinguish AMG from other types of antibiotics.

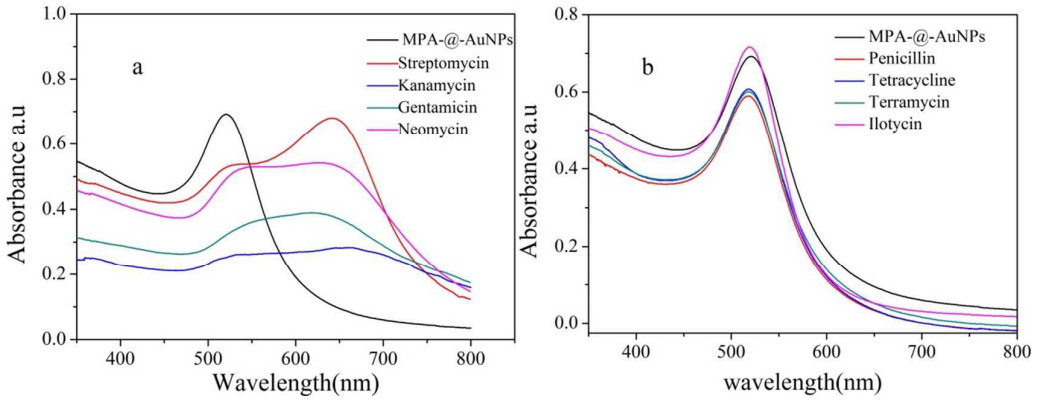

Fig. 7.UV -vis spectra of the PMMA-@-Au NPs after addition of 15μl of AMGs (a) and other types of antibiotics (b), respectively.

We have confirmed that PMMA-@-Au NPs has a strong chelation with metal ions and generates aggregation, giving rise to obvious color change[14]. If the sample was mixed with metal ions, it would disturb the determination of AMGs only by naked eyes. As strong chelating agent of metal ions, EDTA has been confirmed by us that

can screen the interaction of PMMA-@-Au NPs with metal ions. Taking Pb^{2+} as an example (Fig. 8), it makes the transverse SPR of PMMA-@-Au NPs redshift to 542nm (Fig. 8b) and the solution turns to purple (Fig. 8b') suspension due to an induced aggregation. After added EDTA, the UV-vis spectra of mixed solution shows a blue shift to 532nm (Fig. 8c) and the color return to red (Fig. 8c'), indicating that the EDTA extract Pb^{2+} from aggregation of PMMA-@-Au NPs. Finally, the long-wavelength plasmon band appears (Fig. 8e) and the solution turns blue (Fig. 8e') after added 10μl or more streptomycin. The similar results are observed in other samples of AMGs, which demonstrate that the interference from metal ions to determinate AMGs can be eliminated by adding EDTA.

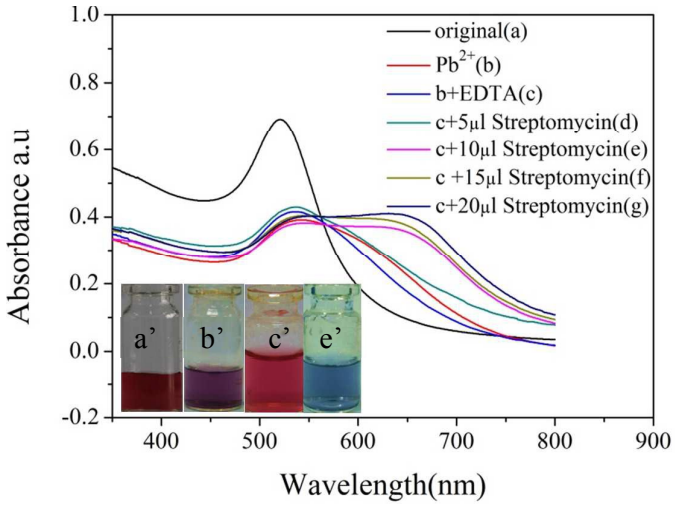

Fig. 8. UV-vis spectra of PMAA-@-Au NPs(a), a in the presence of 400μM Pb^{2+}(b), adding EDTA in b (c), and adding streptomycin in c (d) and its corresponding solution color (a', b', c' and d').

Conclusions

In summary, the self-assembly driven colorimetric method is present to detect AMGs by induced nanochain formation of PMMA-@-Au NPs. The AMGs can serve as molecular linkers to drive PMMA-@-Au NPs with chain-like arrays via an electrostatic dipole interaction, giving rise to obvious color change from red to blue for their colorimetric detection. The test method has many advantages, such as

cost-effective, on-site, read-out by naked eyes and high sensitivity and selectivity, etc. Moreover, the stable chain-like nanostructure comprising drug and polymer functional Au NPs, with intriguing optics and surface properties, is worthy of further investigation for biomedical applications such as cell-imaging, photo-thermal therapy of cancer and controlled release.

Acknowledgment

The authors gratefully acknowledge the financial support from the National Natural Science Foundation of China (No.51103035 and 51403055) and Scientific and Technological Projects of Henan province (132102310422).

1. A. Losoya-Leal, M. C. Estevez, S. O. Martínez-Chapa and L. M. Lechuga, *Talanta*, 2015, 141, 253-258.
2. T. Christian, R. J. Schneider, H. A. Färber, D. Skutlarek, M. T. Meyer and H. E. Goldbach, *CLEAN - Soil, Air, Water*, 2003, 31, 36-44.
3. F. Conzuelo, M. Gamella, S. Campuzano, A. J. Reviejo and J. M. Pingarrón, *Anal. Chim. Acta*, 2012, 737, 29-36.
4. Y. Luo, J. Xu, Y. Li, H. Gao, J. Guo, F. Shen and C. Sun, *Food Control*, 2015, 54, 7-15.
5. J. F. Prescott, *Can.Vet.J.*, 1999, 40, 199-199.
6. Y. Zhang, S. Lu, W. Liu, C. Zhao and R. Xi, *J. Agric. Food Chem.*, 2007, 55, 211-218.
7. S.-H. Chen, Y.-C. Liang and Y.-W. Chou, *J. Sep. Sci.*, 2006, 29, 607-612.
8. M. E. Dasenaki and N. S. Thomaidis, *Anal. Bioanal. Chem.*, 2015, 407, 4229-4245.
9. M. Horká, M. Tesařová, P. Karásek, F. Růžička, V. Holá, M. Sittová and M. Roth, *Anal. Chim. Acta*, 2015, 868, 67-72.
10. D. Liu, Z. Wang and X. Jiang, *Nanoscale*, 2011, 3, 1421-1433.
11. K. Ai, Y. Liu and L. Lu, *J. Am. Chem. Soc.*, 2009, 131, 9496-9497.
12. C. Radhakumary and K. Sreenivasan, *Colloids Surf., A*, 2014, 443, 326-330.
13. P. Tiwari, K. Vig, V. Dennis and S. Singh, *Nanomaterials*, 2011, 1, 31-63.
14. J. Li, C. Han, W. Wu, S. Zhang, J. Guo and H. Zhou, *New J. Chem.*, 2014, 38, 717-722.
15. K. Saha, S. S. Agasti, C. Kim, X. N. Li and V. M. Rotello, *Chem. Rev.*, 2012, 112, 2739-2779.
16. S. J. Tan, M. J. Campolongo, D. Luo and W. Cheng, *Nat Nano*, 2011, 6, 268-276.
17. C. Hamon, S. Novikov, L. Scarabelli, L. Basabe-Desmonts and L. M. Liz-Marzán, *ACS Nano*, 2014, 8, 10694-10703.
18. S. Linic, P. Christopher and D. B. Ingram, *Nat. Mater.*, 2011, 10, 911-921.
19. S. J. Barrow, A. M. Funston, X. Wei and P. Mulvaney, *Nano Today*, 2013, 8, 138-167.
20. Y. Liu, X. Han, L. He and Y. Yin, *Angew. Chem. Int. Ed.*, 2012, 51, 6373-6377.
21. C. Fernández-López, L. Polavarapu, D. M. Solís, J. M. Taboada, F. Obelleiro, R. Contreras-Cáceres, I. Pastoriza-Santos and J. Pérez-Juste, *ACS Appl. Mater. Interfaces*, 2015,

DOI: 10.1021/am5087209.

22. S. Linic, U. Aslam, C. Boerigter and M. Morabito, *Nat. Mater.*, 2015, 14, 567-576.
23. T. Søndergaard, S. M. Novikov, T. Holmgaard, R. L. Eriksen, J. Beermann, Z. Han, K. Pedersen and S. I. Bozhevolnyi, *Nat. Commun.*, 2012, 3, 969.
24. K. J. Savage, M. M. Hawkeye, R. Esteban, A. G. Borisov, J. Aizpurua and J. J. Baumberg, *Nature*, 2012, 491, 574-577.
25. L. Jiang, Y. Sun, F. Huo, H. Zhang, L. Qin, S. Li and X. Chen, *Nanoscale*, 2012, 4, 66-75.
26. I. Tokarev and S. Minko, *Soft Matter*, 2012, 8, 5980-5987.
27. M. Grzelczak, J. Vermant, E. M. Furst and L. M. Liz-Marzán, *ACS Nano*, 2010, 4, 3591-3605.
28. S. Gwo, M.-H. Lin, C.-L. He, H.-Y. Chen and T. Teranishi, *Langmuir*, 2012, 28, 8902-8908.
29. S. Si, A. Kotal and T. K. Mandal, *J. Phys. Chem. C*, 2007, 111, 1248-1255.
30. J. A. Jenkins, Y. Zhou, S. Thota, X. Tian, X. Zhao, S. Zou and J. Zhao, *J. Phys. Chem. C*, 2014, 118, 26276-26283.
31. K.-L. Lee, P.-W. Chen, S.-H. Wu, J.-B. Huang, S.-Y. Yang and P.-K. Wei, *ACS Nano*, 2012, 6, 2931-2939.
32. X. Han, Y. Liu and Y. Yin, *Nano Lett.*, 2014, 14, 2466-2470.
33. D. Perez-Fernandez, D. Shcherbakov, T. Matt, N. C. Leong, I. Kudyba, S. Duscha, H. Boukari, R. Patak, S. R. Dubbaka, K. Lang, M. Meyer, R. Akbergenov, P. Freihofer, S. Vaddi, P. Thommes, V. Ramakrishnan, A. Vasella and E. C. Böttger, *Nat. Commun.*, 2014, 5.
34. H. Chen, W. Hu and C. M. Li, *Sens. Actuators, B*, 2015, 215, 421-427.
35. A. Fernández-Lodeiro, J. Fernández-Lodeiro, C. Núñez, R. Bastida, J. L. Capelo and C. Lodeiro, *ChemistryOpen*, 2013, 2, 200-207.
36. J. B. Li, S. J. Zhang, J. Liang, W. L. Wu, J. W. Guo and H. Y. Zhou, *RSC Adv.*, 2015, 5, 7994-8001.
37. M. S. Young, K. van Tran, E. Goh and J. C. Shia, *J. AOAC Int.*, 2014, 97, 1737-1741.
38. X. Cui, P. Zhang, X. Yang, M. Yang, W. Zhou, S. Zhang, H. Gao and R. Lu, *Anal. Chim. Acta*, 2015, 878, 131-139.
39. N. Derbyshire, S. J. White, D. H. J. Bunka, L. Song, S. Stead, J. Tarbin, M. Sharman, D. Zhou and P. G. Stockley, *Anal. Chem.*, 2012, 84, 6595-6602.
40. L. R. Schoukroun-Barnes, S. Wagan and R. J. White, *Anal. Chem.*, 2014, 86, 1131-1137.
41. X. Shen, L. Chen, D. Li, L. Zhu, H. Wang, C. Liu, Y. Wang, Q. Xiong and H. Chen, *Acs Nano*, 2011, 5, 8426-8433.
42. C. Fang, Y. Fan, J. M. Kong, Z. Q. Gao and N. Balasubramanian, *Appl. Phys. Lett*, 2008, 92.
43. Z. Nie, A. Petukhova and E. Kumacheva, *Nat Nano*, 2010, 5, 15-25.
44. N. Vragović, D. Bažulić and B. Njari, *Food Chem. Toxicol.*, 2011, 49, 352-355.
45. S. Srivastava and N. A. Kotov, *Soft Matter*, 2009, 5, 1146-1156.